Available online at www.sciencedirect.com
ScienceDirect
Physica A 385 (2007) 439–455
PHYSICA A
www.elsevier.com/locate/physa

Mapping from a fragile glass-forming system to a simpler one near their glass transitions

Michio Tokuyama[a,*], Takayuki Narumi[b], Eri Kohira[b]

[a]*Institute of Fluid Science, Tohoku University, Sendai 980-8577, Japan*
[b]*Department of Mechanical Engineering, Tohoku University, Sendai 980-8579, Japan*

Received 16 April 2007; received in revised form 22 May 2007
Available online 19 July 2007

Abstract

Extensive molecular-dynamics simulations on two different glass-forming systems are performed to test the prediction proposed recently by the mean-field theory (MFT) of glass transition that a fragile system can be mimicked by a simpler one near their glass transitions. One is a simulation for a hard-sphere fluid with size polydispersity where the volume fraction ϕ is a control parameter and the other is for a Lennard-Jones binary mixture where the inverse temperature $1/T$ is a control parameter. Then, their mean-square displacements are fully analyzed by MFT. Thus, we show that both results are collapsed on a master curve given by MFT when $D_S^L(\phi) = D_S^L(T)$, where D_S^L is a long-time self-diffusion coefficient. We also investigate the non-singular behavior of D_S^L consistently from a unified standpoint based on MFT. Thus, we show that macroscopic physical quantities in a fragile system can be transformed into those in a simpler one through a universal parameter D_S^L.

Keywords: Glass transition; Hard-sphere fluid; Lennard-Jones binary mixture; Long-time self-diffusion coefficient; Mean-field theory; Mean-square displacement; Universality

1. Introduction

Study of glass formation is one of the pioneering works in condensed matters physics. Despite decades of many researches, our understanding of the glass transition from liquid to glass is still incomplete. Nevertheless, considerable attention has been drawn to universal features in various complex systems near the glass transitions [1–5].

In order to study the long-lived spatial heterogeneities in suspensions of hard-sphere colloids near the colloidal glass transition [6], Tokuyama [7] has derived the nonlinear stochastic diffusion equation for the density fluctuation. By employing the fact that the non-Gaussian parameter is negligible even near the colloidal glass transition, he has then derived a nonlinear mean-field equation for the particle mean-square displacement from that stochastic equation [8]. According to this idea, substantial extensions were made to

*Corresponding author. Tel./fax: +81 22 217 5327.
E-mail addresses: tokuyama@fmail.ifs.tohoku.ac.jp, tokuyama@ifs.tohoku.ac.jp (M. Tokuyama).

0378-4371/$ - see front matter © 2007 Elsevier B.V. All rights reserved.
doi:10.1016/j.physa.2007.07.007

study not only the slow dynamics of colloidal suspensions, but also that of molecular systems near the glass transition, leading to the mean-field theory (MFT) [9–13]. The essential points of MFT are as follows [12,13]:

(i) The mean-square displacement obeys the nonlinear mean-field equations, which describe not only the slow dynamics of colloidal suspensions but also that of the molecular systems near the glass transition. Those equations contain two unknown coefficients, the mean-free path $\ell(p)$ and the long-time self-diffusion coefficient $D_S^L(p)$, where p is a control parameter, such as a volume fraction and an inverse temperature.
(ii) The mean-free path ℓ, within which the particles can move freely without any interactions, is obtained by fitting the mean-field equations with experiments and simulations. It is shown to be uniquely determined by D_S^L only.
(iii) The long-time self-diffusion coefficient D_S^L, which results from the long-time correlation effect due to the many-body interactions between particles, is obtained by the fitting with experiments and simulations. First, the fitting results are used to find a singular function of p, which can partially describe the experiments and the simulations. The singular function contains two unknown coefficients, a singular point p_c and a positive constant ε. Both coefficient are determined by the fitting, where p_c depends on the details of many-body interactions, such as polydispersity, while ε is constant if the main interactions are the same in different systems. The singular function deviates from the fitting values at higher values of p. Hence a non-singular function of p is then obtained from the singular function by introducing a transformation from p to a new variable p_n, which contains an unknown coefficient α. This can describe the experiments and the simulations very well, where α is constant if the main interactions are the same in different systems.
(iv) D_S^L is a universal parameter. At a given value of D_S^L, the macroscopic physical quantities in any systems become identical with each other. Hence one can map the dynamics in one system onto another consistently. This suggests that the dynamics of a fragile system can be predicted by that of a simpler system.

In this paper, we perform the extensive molecular-dynamics simulations on two different systems, hard-sphere fluids and Lennard-Jones binary mixtures. Thus, we demonstrate the essential points (i)–(iv) discussed above by analyzing those simulations by MFT, in addition to the previous related works.

The paper is organized as follows. In Section 2 we briefly describe the MFT. In Section 3 we analyze the simulation results on two different systems by MFT, the hard-sphere fluids and the Lennard-Jones binary mixtures. In Section 4 we discuss the dynamical mapping from one system to another at a given value of D_S^L. We conclude in Section 5 with a summary.

2. Mean-field theory

In this section, we briefly summarize and discuss the MFT recently proposed [8,12], which consists of the following two essential points: (A) a nonlinear mean-field equation for the mean-square displacement, and (B) a non-singular long-time self-diffusion coefficient. Next we discuss those separately.

2.1. Mean-field equations

We consider a three-dimensional equilibrium system surrounded by the heat bath with temperature T, in which there exist N particles of interest with mass m and radius a in the volume V. Then, the mean-square displacement $M_2(t)$ is given by

$$M_2(t) = \frac{1}{N}\sum_{i=1}^{N}\langle[\boldsymbol{X}_i(t) - \boldsymbol{X}_i(0)]^2\rangle, \tag{1}$$

where $\boldsymbol{X}_i(t)$ denotes a position vector of ith particle and the brackets, the equilibrium ensemble average. Then, the MFT shows that the slow dynamics of the molecular systems near the glass transition can be described by the following nonlinear equation for the mean-square displacement $M_2(t)$:

$$\frac{\mathrm{d}}{\mathrm{d}t}M_2(t) = 2dD_S^L(p) + 2d\left[\frac{v_0^2}{d}t - D_S^L(p)\right]\mathrm{e}^{-M_2(t)/\ell^2} \tag{2}$$

with the long-time self-diffusion coefficient $D_S^L(p)$ and the mean-free path $\ell(p)$, where p is a control parameter, such as a volume fraction ϕ and an inverse temperature $\beta(=1/T)$, $v_0(=(dk_BT/m)^{1/2})$ the average velocity of a particle, and d a spatial dimensionality. Here the mean-free path $\ell(p)$ is a length in which a particle can move freely without any interactions between particles and can be determined by a fitting with data.

The formal solution of Eq. (2) is given by

$$M_2(t) = 2dD_S^L t + \ell^2 \ln\left[\mathrm{e}^{-2\,dt/\tau_\beta} + \frac{1}{2d^2}\left(\frac{\tau_\beta}{\tau_f}\right)^2\left\{1 - \left(1 + 2d\frac{t}{\tau_\beta}\right)\mathrm{e}^{-2\,dt/\tau_\beta}\right\}\right], \tag{3}$$

where $\tau_\beta(=\ell^2/D_S^L)$ denotes a time for a particle to diffuse over a distance of order ℓ with the diffusion coefficient D_S^L, and $\tau_f(=\ell/v_0)$ is a free time during which each particle can move freely without any interactions between particles. As discussed in Ref. [13], by introducing the dimensionless variables $\hat{\boldsymbol{X}} = \boldsymbol{X}/a$ and $\hat{t} = t/t_0$, the solution (3) is written as

$$\hat{M}_2(t) = 6\hat{D}_L\hat{t} + \hat{\ell}^2 \ln\left[\mathrm{e}^{-6\hat{D}_L\hat{t}/\hat{\ell}^2} + \frac{1}{18}\left(\frac{\hat{\ell}}{\hat{D}_L}\right)^2\left\{1 - \left(1 + 6\frac{\hat{D}_L\hat{t}}{\hat{\ell}^2}\right)\mathrm{e}^{-6\hat{D}_L\hat{t}/\hat{\ell}^2}\right\}\right], \tag{4}$$

where $\hat{D}_L = D_S^L/av_0$, $\hat{\ell} = \ell/a$, $t_0 = a/v_0$, and $d = 3$ here. From Eq. (4), one can find the following asymptotic forms:

$$M_2(t) \simeq \begin{cases} \hat{t}^2 & \text{for } \hat{t} \ll 1, \\ 6\hat{D}_L(p)\hat{t} & \text{for } \hat{t} \gg 1. \end{cases} \tag{5}$$

As discussed in Ref. [13], for intermediate times, $M_2(t)$ obeys a logarithmic growth and a power-law growth of a super-diffusion type with two different characteristic times, a caging time t_γ and a β-relaxation time t_β.

We should note here that in the present paper the length is scaled by radius a and the velocity is scaled by the average velocity $v_0(=(dk_BT/m)^{1/2})$, although in Ref. [13], those are scaled by diameter σ and the velocity $(k_BT/m)^{1/2}$, respectively. This scaling is rather reasonable because only under such a scaling the ratio of the long-time self-diffusion coefficient D_S^L in the monodisperse hard-sphere fluid to that in the suspension of monodisperse hard spheres without hydrodynamic interactions coincides with the short-time self-diffusion coefficient D_S^S caused by the hydrodynamic interactions [11]. Hence all the length and the average velocity in the molecular systems discussed in Ref. [13] must be rescaled by them. This is done by just replacing $\hat{D}_L$ by $(2/\sqrt{3})\hat{D}_L$ and does not cause any serious quantitative corrections to the previous results obtained for the molecular systems.

The mean-square displacements of simulations are first analyzed by using Eq. (4). Thus, two unknown parameters $\hat{D}_L(p)$ and $\hat{\ell}(p)$ are found by fitting the mean-field results with simulations and then $\hat{\ell}$ is shown to be a function of $\hat{D}_L$. Hence the time evolution of $\hat{M}_2(t)$ is shown to depend only on $\hat{D}_L(p)$.

As shown in Ref. [13], as p is increased, the supercooled state and the glassy state appear at p_β (or $\hat{D}_\beta$) and p_g (or $\hat{D}_g$), respectively, where $p_g > p_\beta$ ($\hat{D}_g < \hat{D}_\beta$). Here the experiment of the colloidal suspension [14] suggests that $\hat{D}_\beta \simeq 2.9512 \times 10^{-3} (\simeq 10^{-2.530})$ at $\phi_\beta \simeq 0.544$ and $\hat{D}_g \simeq 9.1622 \times 10^{-6} (\simeq 10^{-5.038})$ at $\phi_g \simeq 0.580$. As discussed in Ref. [13], these values might be universal and be used to determine p_β and p_g in the other systems.

2.2. A non-singular long-time self-diffusion coefficient

We next discuss another important prediction by MFT [12]. It is a prediction that the experimental and the simulation results for the long-time self-diffusion coefficient can be approximately described by a singular function

$$\frac{D_L^S(p)}{\Delta_0} = \frac{D_S^S(p)}{D_0}\frac{1 - Cp}{1 + \varepsilon(D_S^S/D_0)(p/p_c)(1 - p/p_c)^{-2}}, \tag{6}$$

where p_c is a singular point caused by the many-body interactions between particles and ε a positive coefficient to be determined. The singular part in the denominator of Eq. (6) results from the long-time correlation effect due to the many-body interactions between particles. Here $D_S^S(p)$ is the short-time self-diffusion coefficient, D_0 a single-particle diffusion constant, C the long-time coupling effect between different interactions, and $\Delta_0 = D_0$ for the suspensions and $\Delta_0 = av_0$ for the molecular systems. For the suspensions of hard spheres the theoretical result for $D_S^S(\phi)/D_0$ is given by Eq. (11) of Ref. [15], where $C(= 9/32)$ is the coupling effect between the hydrodynamic interactions and the direct interactions. On the other hand, for all molecular systems, $D_S^S(p)/D_0 = 1$ and $C = 0$, except the hard-sphere fluids, where $D_S^S(\phi)/D_0$ is given by Eq. (11) of Ref. [15] (see Ref. [11] for details). As shown in the next section, the value of ε depends on the systems but does not depend on the details of the long-time many-body interactions, such as a polydispersity, while p_c depends on those details.

The experimental and simulation results deviate from the singular function given by Eq. (6) at higher values of p and obey rather a non-singular function of p [12]. We next derive it by using Eq. (6). As discussed in Refs. [9,10], in order to avoid a singular part in Eq. (6), we introduce a transformation from p to a new variable p_n by

$$p_n = p + 10^{-\alpha}\frac{p}{p_c(p_c - p)}, \tag{7}$$

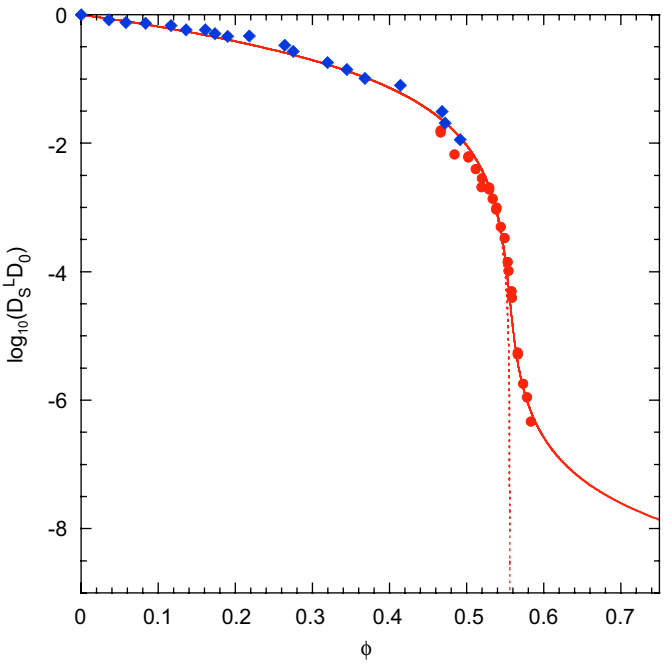

Fig. 1. (Color online) A log plot of $D_S^L(\phi)/D_0$ versus ϕ. The circles indicate the experimental results from Ref. [14]. The dotted line indicates the singular function given by Eq. (6) and the solid line the non-singular function given by Eq. (6) with Eq. (7), where $\varepsilon = 1$, $\alpha \simeq 4.86$, $\phi_c \simeq 0.556$, and $C \simeq 9/32$.

where α is a positive constant to be determined. Solving Eq. (7) for p and inserting it into Eq. (6), one can thus determine the coefficient α so that $D_S^L(p_n)$ fits the experimental and simulation results. As shown in the next section, α depends on the system but does not depend on the details of the long-time many-body interactions, such as a polydispersity. In Fig. 1, the experimental data for the suspension of dense neutral colloids with the 6% size polydispersity [14] are shown versus the volume fraction ϕ, where $\phi_c \simeq 0.556$, $\alpha \simeq 4.86$, and $C \simeq 9/32$. Here the main mechanisms are hydrodynamic interactions between particles and direct interactions between particles. The data deviate from the singular function given by Eq. (6) at higher volume fractions and are described by the non-singular function given by Eq. (6) with Eq. (7) very well. As shown in the next section, this value of α is the same as that in hard-sphere fluids, where only the direct interactions exist.

3. Analyses of simulation data by MFT

In this section, we analyze the simulation data for the mean-square displacements by employing the MFT. We study two different molecular systems, hard-sphere fluids with different size polydispersities and Lennard-Jones binary mixtures.

3.1. Hard-sphere fluids

We first analyze the simulation data for hard-sphere fluids.

The system consists of 10 976 hard spheres with radius a_i and mass m_i in a cubic box of volume V at a constant temperature T, where the distribution of radii obeys a Gaussian distribution with standard deviation s divided by the average radius a, and mass m_i is proportional to a_i^3. Then, the control parameter is the volume fraction given by $\phi = (4\pi a^3 N/3V)(1 + 3s^2)$. The mechanism of this system is only a direct interaction between particles. Let $\boldsymbol{V}_i(t)$ be a velocity of ith particle. Then, the motion of ith particle is described by the Newton equation

$$m_i \frac{\mathrm{d}}{\mathrm{d}t} \boldsymbol{V}_i(t) = \sum_{j \neq i} \boldsymbol{F}(\boldsymbol{X}_{ij}), \tag{8}$$

where $\boldsymbol{F}(\boldsymbol{X}_{ij})$ denotes the force due to the elastic binary collisions between particles i and j, and $\boldsymbol{X}_{ij} = \boldsymbol{X}_i - \boldsymbol{X}_j$. We first scale the position vector $\boldsymbol{X}_i$ with radius a, time t with t_0, and D_S^L with av_0. Then, we solve Eq. (8) under a periodic boundary condition and appropriate initial conditions together with the momentum and the energy conservation laws. The simulations start from disordered initial states which are obtained by using the Jodrey and Tory's [20] algorithm. We first wait for a long time which is enough to reach a final state where the mean-square displacement $M_2(t)$ grows linearly in time. By choosing this final state as an initial state, we then repeat the simulations again until the whole time behavior of $M_2(t)$ coincides with a previous one. The whole time is counted as a waiting time to reach an equilibrium. We discuss the following three cases where the polydispersity is given by $s = 0, 0.06$, and 0.15. The waiting time is of order $10^5 t_0$. Here the simulation data for $s = 0.06$ are taken from Refs. [18,19].

Depending on the value of s, the system shows different phases for higher volume fractions. When $s = 0$, the crystallization occurs for $\phi > 0.535$, showing a first-order phase transition. When $s = 0.15$, no crystallization occurs at any volume fractions, leading to a glass transition for higher volume fractions. On the other hand, when $s = 0.06$, re-entrant melting (transition from crystal to supercooled liquid) followed by a glass transition occurs temporarily within a waiting time of order $10^5 t_0$ but the crystallization finally starts to occur for much longer waiting times of order $2 \times 10^5 t_0$ [19]. From a stand point based on the MFT [13], the supercooled point over which the supercooled state appears is suggested as $\log_{10}(\hat{D}_\beta) \simeq -2.530$ and the glass transition point is $\log_{10}(\hat{D}_g) \simeq -5.038$. From this point, there are three phases in the system with $s = 0.15$; a liquid phase [L] for $\phi < \phi_\beta (\simeq 0.5611)$, a supercooled liquid phase [S] for $\phi_\beta \leqslant \phi < \phi_g (\simeq 0.5981)$, and a glass phase [G] for $\phi_g \leqslant \phi$. Here the phases in the system with $s = 0.06$ were already discussed in Ref. [19].

In Fig. 2, the mean-square displacement $M_2(t)$ is shown for different volume fractions at $s = 0$, 0.06, and 0.15 together with the mean-field results given by Eq. (4). Within error, one can fit the mean-field results with

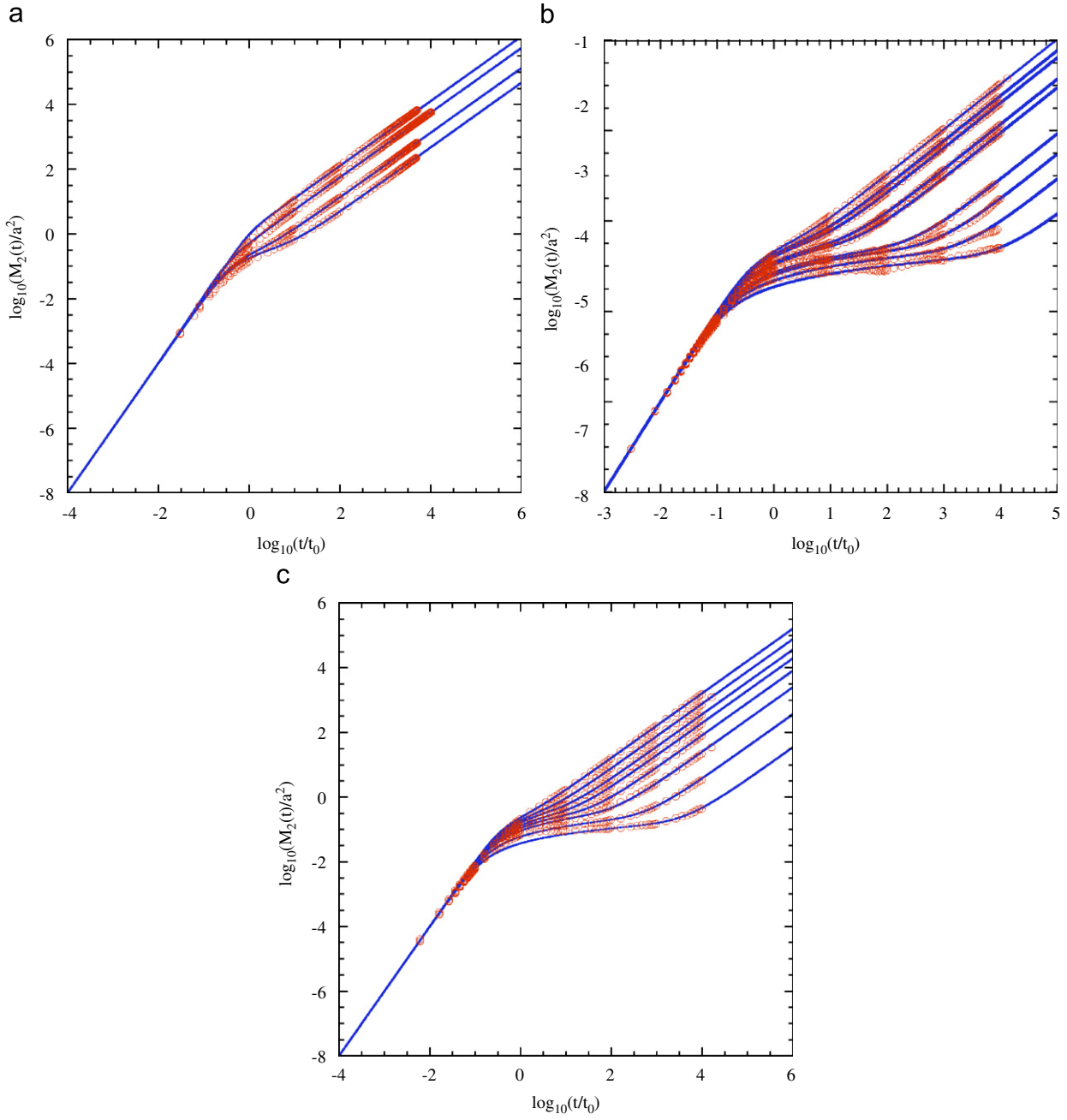

Fig. 2. (Color online) A log–log plot of $M_2(t)$ versus time at different polydispersities. The symbols indicate the simulation results and the solid lines the mean-field results given by Eq. (4). (a) $s = 0$ for $\phi = 0.30, 0.40, 0.50$, and 0.535 (from left to right), (b) $s = 0.06$ for $\phi = 0.51$, 0.53, 0.54, 0.5575, 0.56, 0.5780, 0.58, 0.586, and 0.6 (from left to right), and (c) $s = 0.15$ for $\phi = 0.50$, 0.53, 0.55, 0.56, 0.57, 0.58, 0.59, and 0.60 (from left to right).

the simulation results well by adjusting the mean-free path ℓ appropriately, except a highly supercooled state and a glassy state for $\phi \geqslant \phi_c$. In such states, the MFT does not fit with the simulation results because it can describe only the dynamics of the system in equilibrium but the system is still in a metastable state, approaching to an equilibrium state very slowly.

In Fig. 3, the fitting results for the long-time self-diffusion coefficient $D_S^L(\phi)$ are plotted at different values of s. As discussed in Refs. [11,12], the simulation results can be partially described by the

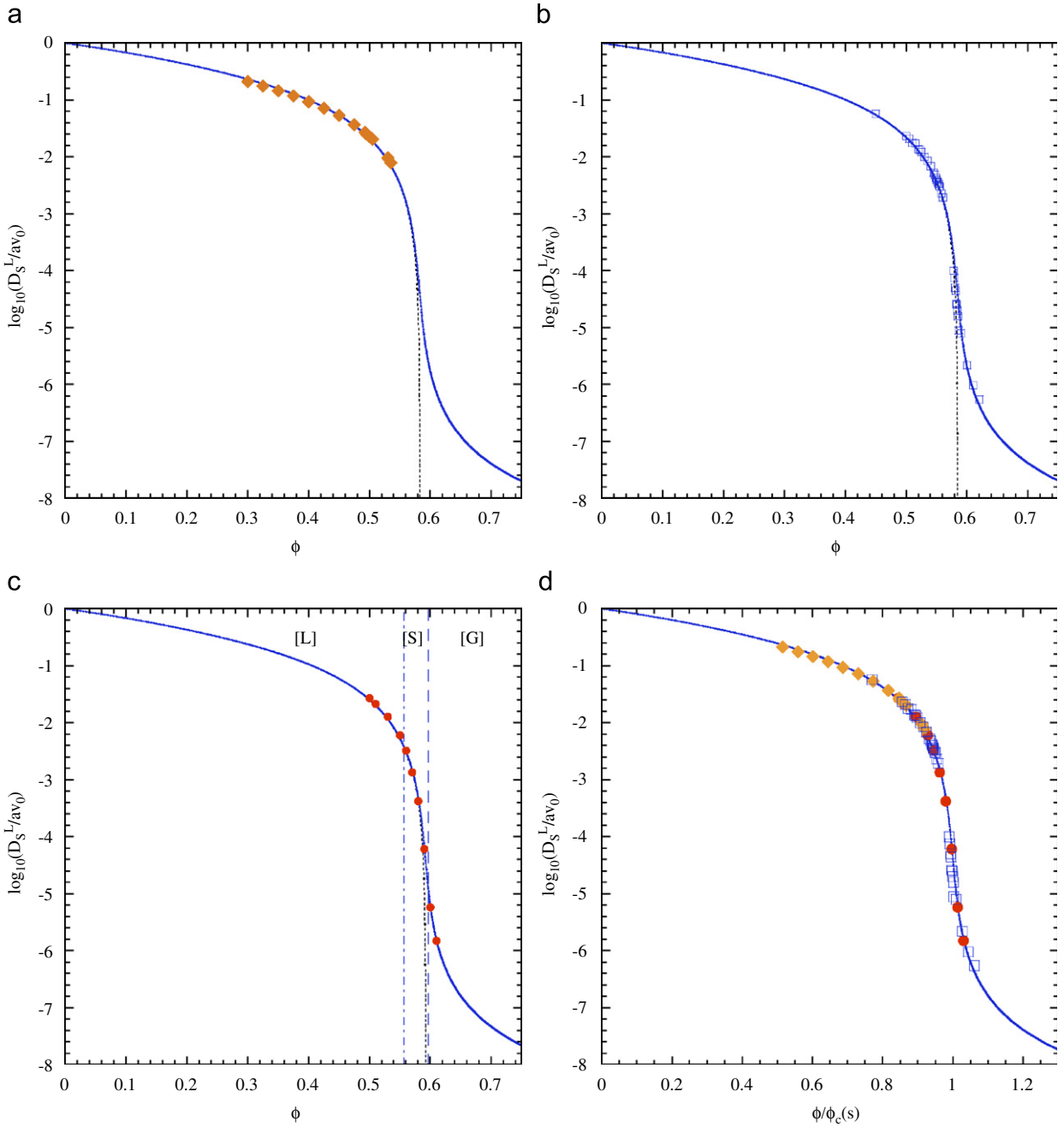

Fig. 3. (Color online) A log plot of $D_S^L(\phi)$ versus ϕ for different polydispersities; (a) $s = 0$, (b) 0.06, and (c) 0.15. The symbols indicate the simulation results, the solid lines the non-singular function given by Eq. (9) with Eq. (12), and the dotted lines the singular function given by Eq. (9). The vertical dot-dashed line indicates $\hat{D}_\beta$ and the vertical dotted line $\hat{D}_g$. (d) A log plot of $D_S^L(\phi)$ versus $\phi/\phi_c(s)$ for all polydispersities.

singular function

$$\frac{D_S^L(\phi)}{av_0} = \frac{D_S^S(\phi)}{D_0} \frac{1}{1 + \varepsilon(D_S^S/D_0)(\phi/\phi_c(s))(1 - \phi/\phi_c(s))^{-2}}, \tag{9}$$

where $C = 0$ and $\varepsilon = 1$. The reason why the short-time self-diffusion coefficient $D_S^S(\phi)$ should appear in Eq. (9) was fully discussed in Refs. [11,19]. This is needed to fit Eq. (9) with the simulation results even at lower volume fractions. Near ϕ_c, however, Eq. (9) reduces to

$$\frac{D_S^L(\phi)}{av_0} \propto \left(1 - \frac{\phi}{\phi_c}\right)^2. \tag{10}$$

Then, D_S^L does not depend on D_S^S near ϕ_c. Hence one may take $D_S^S/D_0 = 1$ for intermediate volume fractions as in the other molecular systems. The singular point $\phi_c(s)$ depends on s and is given by

$$\phi_c(0) \simeq 0.5828, \quad \phi_c(0.06) \simeq 0.5845, \quad \phi_c(0.15) \simeq 0.5923. \tag{11}$$

Here we note that the effect of the polydispersity on D_S^L appears only in the singular point ϕ_c because the mechanisms in the systems are the same as each other, irrespective of polydispersities. The simulation results for $s = 0.06$ and 0.15 start to deviate from such a singular function at higher volume fractions and are well described by the non-singular functions discussed in Ref. [19], where for $s = 0$ no result exists for $\phi > 0.535$ because of crystallization. In fact, the non-singular function can be obtained by introducing a transformation from ϕ to a new variable ϕ_n by

$$\phi_n = \phi + 10^{-\alpha} \frac{\phi}{\phi_c(\phi_c - \phi)}. \tag{12}$$

Here α is a positive constant and is determined so that Eq. (9) can fit the simulation results. In fact, we find for all values of s

$$\alpha \simeq 4.86. \tag{13}$$

If D_S^L is plotted versus $\phi/\phi_c(s)$, therefore, all simulation results are collapsed on only one non-singular curve. This is shown in Fig. 3(d). We note here that α does not depend on s and is the same as that in the suspension of colloids. Hence, the experimental data are also collapsed on the same curve as that in Fig. 3(d) if those data are divided by $1 - C\phi$, where $C = 9/32$. Thus, the value of α is determined by only the direct interactions.

By fitting the solution (4) with the simulation results, one can also obtain the fitting values of the mean-free path ℓ. In Fig. 4, ℓ/ℓ_0 is shown at different polydispersities, where ℓ_0 is a fundamental length in the system. As discussed in Ref. [13], ℓ/ℓ_0 is determined by $\hat{D}_L$ only, irrespective of the polydispersity s. In fact, all data seem to be collapsed on a single curve within error. This is reasonable because $\hat{D}_L$ indicates the long-time correlation effect due to the many-body interactions between particles and hence the average spatial structures in different systems are considered to be identical with each other at the given value of $\hat{D}_L$, leading to the same mean-free path. Hence all the simulation results for $M_2(t)$ obey a master curve given by Eq. (4) at a given value of $\hat{D}_L$ (see Section 4).

Finally, we discuss the universal nature for the pressure P. In the hard-sphere fluids, the pressure is given by

$$\frac{PV}{Nk_BT} = 1 - \frac{2}{3Nk_BT\Delta t} \sum_{collisions} \frac{m_i m_j}{m_i + m_j} \boldsymbol{V}_{ij} \cdot \boldsymbol{X}_{ij}, \tag{14}$$

where the summation is taken over all the collisions occurred in an appropriate unit time Δt, and $\boldsymbol{V}_{ij} = \boldsymbol{V}_i - \boldsymbol{V}_j$. In Fig. 5, the pressure P in the liquid state is plotted versus ϕ for different polydispersities, $s = 0, 0.06$, and 0.15. All data are shown to partially obey the power law

$$\frac{PV}{Nk_BT} = A\left(1 - \frac{\phi}{\phi_{rcp}}\right)^{-B}, \tag{15}$$

where A and B are positive constants to be determined, and ϕ_{rcp} is a random close packing fraction given by 0.64. We note here that the singular behavior given by Eq. (15) is similar to that obtained in the previous simulation results [21–23] but the values of the exponent B are slightly different from theirs. In order to test whether $\hat{D}_L$ is a universal parameter or not, we next plot the pressure P versus $\hat{D}_L$ in Fig. 6. All data are shown to be collapsed on a single curve, which is unknown. Thus, $\hat{D}_L$ is verified to be a universal parameter. For comparison, one of power laws given by Eq. (15) is also plotted by using Eqs. (9) and (12). This power law can

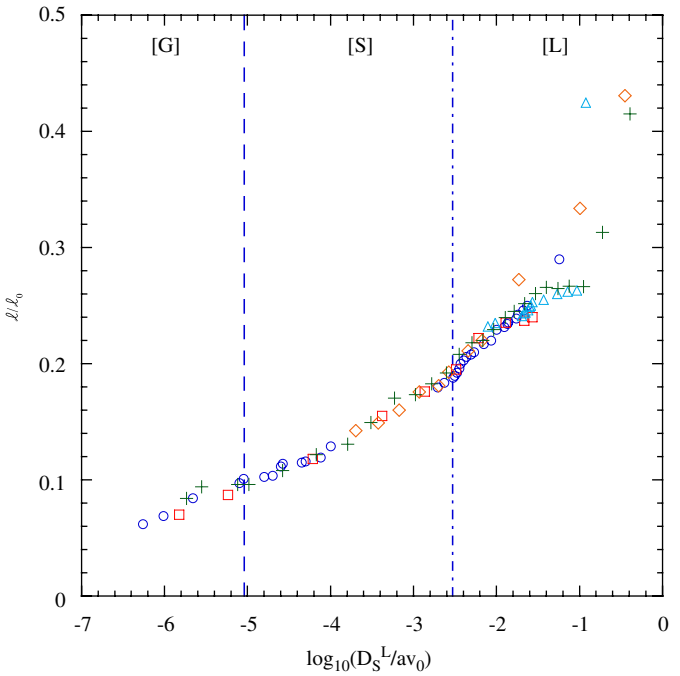

Fig. 4. A plot of the mean-free path ℓ/ℓ_0 versus $\hat{D}_L$. The symbols indicate the fitting values of the mean-free path at $s = 0$ (△), 0.06 (○), and 0.15 (□), where $\ell_0 = a$. The symbols (+) indicate the fitting values of $\hat{\ell}$ for $\hat{M}_2(t)$ in the Lennard-Jones binary mixtures where $\ell_0 = \sigma_{AA}/2$, and the symbols (◇) the fitting values in the confined Lennard-Jones binary mixtures where $\ell_0 = (1.26/0.94)\sigma_{AA}/2$. The vertical dot-dashed line indicates $\hat{D}_\beta$ and the vertical dotted line $\hat{D}_g$.

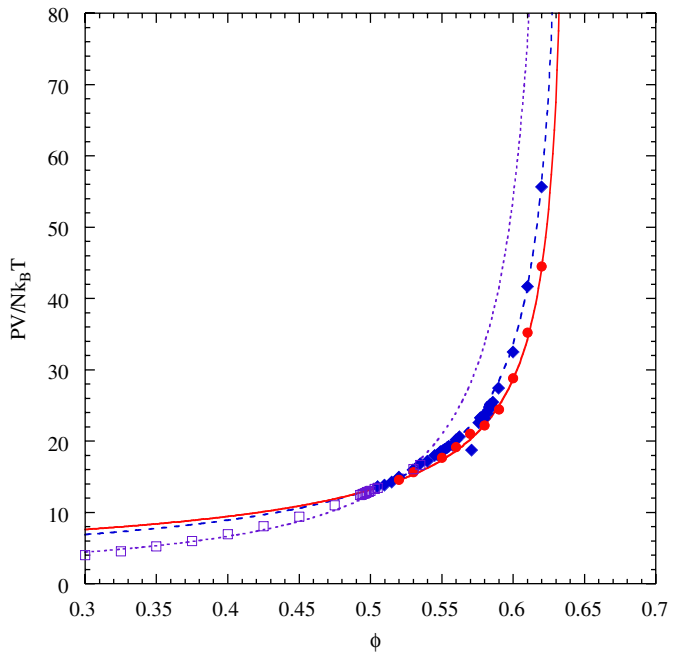

Fig. 5. (Color online) A plot of the pressure P in the liquid state versus ϕ. The symbols indicate the simulation results at $s = 0$ (□), 0.06 (◇), and 0.15 (○). The dotted line indicates the fitting line with $A = 2.1$ and $B = 1.17$, the dashed line with $A = 4.3$ and $B = 0.74$, and the solid line with $A = 5.12$ and $B = 0.62$.

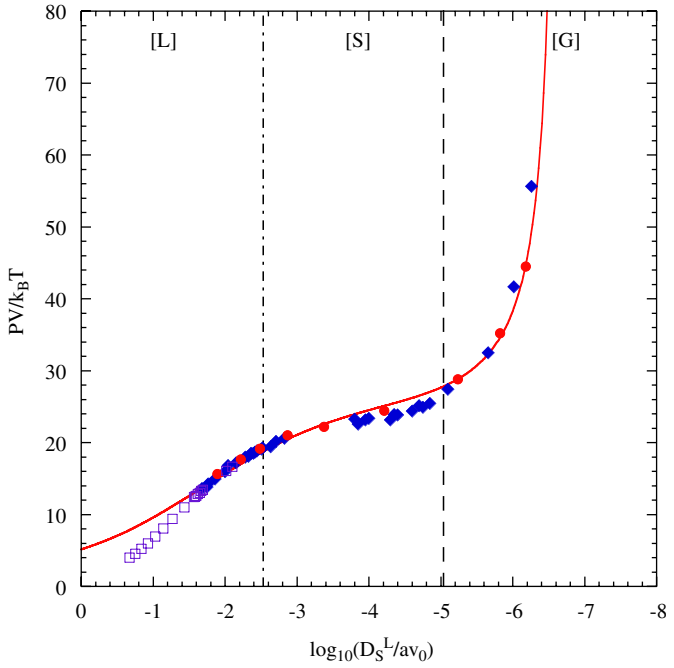

Fig. 6. (Color online) A plot of the pressure P in the liquid state versus D_S^L/av_0. The details are the same as in Figs. 4 and 5. The solid line indicates the power law given by Eq. (15) for $s = 0.15$.

describe well the results for volume fractions higher than 0.5. We note that in the supercooled liquid, the pressure P seems to increase gradually as $\hat{D}_L$ decreases, while in the other states it increases steeply.

3.2. Lennard-Jones binary mixtures

We next analyze the simulation data for Lennard-Jones binary mixtures. Our system contains $N = 10\,976$ particles with mass m, which is composed of $N_A = 8780$ particles of type A and $N_B = 2196$ particles of type B, where $N_A/N \simeq 0.8$. The interaction pair potential is given by

$$U_{\alpha\beta}(r) = 4\varepsilon_{\alpha\beta}\left[\left(\frac{\sigma_{\alpha\beta}}{r}\right)^{12} - \left(\frac{\sigma_{\alpha\beta}}{r}\right)^{6}\right], \tag{16}$$

where indices α, β run on the particle types A and B. The parameters are chosen as in Ref. [16]; $\varepsilon_{AA} = 1.0, \sigma_{AA} = 1.0, \varepsilon_{AB} = 1.5, \sigma_{AB} = 0.8, \varepsilon_{BB} = 0.5$, and $\sigma_{BB} = 0.88$. Let $\boldsymbol{X}_i^{\alpha}(t)$ denote the position vector of ith particle of type α. Then, the ith particle of type α obeys the Newton equation

$$m\frac{\mathrm{d}^2}{\mathrm{d}t^2}\boldsymbol{X}_i^{\alpha}(t) = -\nabla_{\alpha}\sum_{\beta}\sum_{j} U_{\alpha\beta}(\boldsymbol{X}_{ij}^{\alpha\beta}), \tag{17}$$

where $\boldsymbol{X}_{ij}^{\alpha\beta} = \boldsymbol{X}_i^{\alpha} - \boldsymbol{X}_j^{\beta}$. The simulations are performed with the interaction potential cut at $2.5\sigma_{\alpha\beta}$, and the box length of the cubic simulation cell is $20.89\sigma_{AA}$. The average particle distance L_0 is given by $L_0 = 20.89\sigma_{AA}/10\,976^{1/3} = 0.94\sigma_{AA}$. Periodic boundary conditions are used. Length, time, and temperature are scaled by $a(= \sigma_{AA}/2)$, $a/(3\varepsilon_{AA}/m)^{1/2}$, and ε_{AA}/k_B, respectively. The control parameter is an inverse temperature $\beta(= 1/T)$. The Newton equations were solved by the velocity Verlet algorithm. The system was equilibrated via a velocity rescaling procedure at each temperature. The waiting time to equilibrate the system is of order $10^5 t_0$.

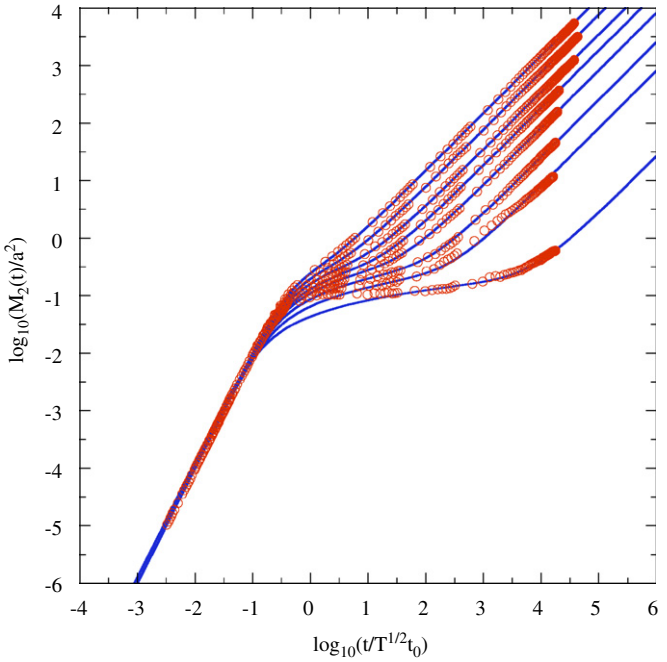

Fig. 7. (Color online) A log–log plot of the mean-square displacement $M_2(t)$ versus time for different temperatures; T (or β) = 1.428 (0.7), 1.0 (1.0), 0.769 (1.3), 0.667 (1.5), 0.588 (1.7), 0.526 (1.9), 0.478 (2.09), and 0.417 (2.4) (from left to right). The open circles indicate the simulation results and the solid lines the mean-field results given by Eq. (4).

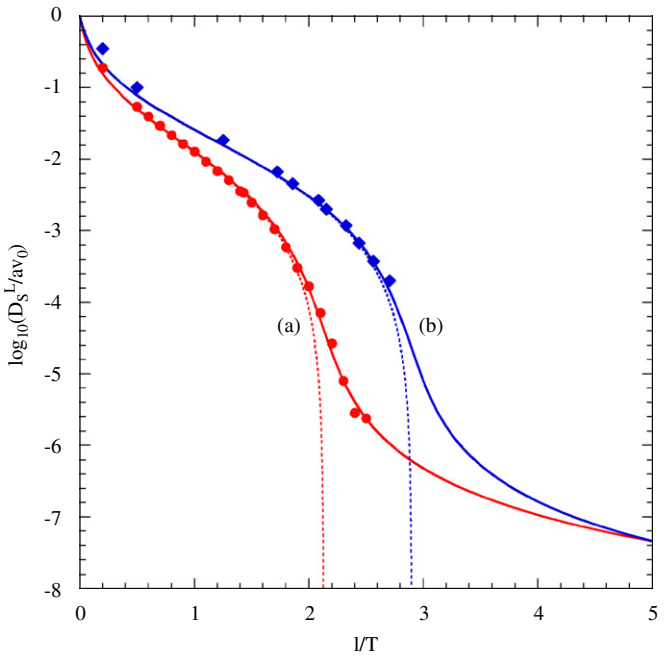

Fig. 8. (Color online) A log plot of the long-time self-diffusion coefficient D_L/av_0 versus $1/T$. The solid line indicates the non-singular function given by Eq. (13) with Eq. (14) and the dotted line the singular function given by Eq. (13). (a) The filled circles indicate the present simulation results for the Lennard-Jones binary mixtures, where $\varepsilon = 46.77$, $\alpha = 2.05$, and $\beta_c \simeq 2.1285 (T_c \simeq 0.4698)$. (b) The filled diamonds indicate the simulation results for the confined Lennard-Jones binary mixtures from Ref. [17], where $\varepsilon = 46.77$, $\alpha = 2.05$, and $\beta_c \simeq 2.9070 (T_c \simeq 0.3440)$.

In Fig. 7, the time evolution of $M_2(t)$ is shown versus the scaled time $t/(T^{1/2}t_0)$ for different temperatures; $T = 1.428$, 1.0, 0.769, 0.667, 0.588, 0.526, 0.478, and 0.417. Within error, one can fit the mean-field results with the simulation results well by adjusting the mean-free path ℓ appropriately, except a highly supercooled state and a glassy state for $\beta \geqslant \beta_c$, where β_c is a singular point discussed below. From this fitting, one can obtain the long-time self-diffusion coefficient $\hat{D}_L$ and the mean-free path $\hat{\ell}$ consistently.

In Fig. 8, a log plot of $\hat{D}_L$ is shown versus $1/T$. From a stand point based on the MFT [13], one can find three phases in this system; a liquid phase [L] for $T > T_\beta$, a supercooled liquid phase [S] for $T_\beta \geqslant T > T_g$, and a glass phase [G] for $T_g \geqslant T$, where $T_\beta \simeq 0.6758$ ($\beta_\beta \simeq 1.4797$) and $T_g \simeq 0.4376$ ($\beta_g \simeq 2.2851$). The simulation results can be partially described by the singular function

$$\frac{D_S^L(\beta)}{av_0} = \frac{1}{1 + \varepsilon(\beta/\beta_c)(1 - \beta/\beta_c)^{-2}}, \tag{18}$$

where $\beta_c \simeq 2.1285$ ($T_c \simeq 0.4698$) and $\varepsilon \simeq 46.77$. Similar to the hard-sphere fluids, the simulation results also deviate from this singular function at lower temperatures and are described by the non-singular functions well. The transformation from β to a new variable β_n is given by

$$\beta_n = \beta + 10^{-\alpha}\frac{\beta}{\beta_c(\beta_c - \beta)}, \tag{19}$$

where $\alpha \simeq 2.05$. Then, the non-singular function can describe the simulation results well within a waiting time of order $2 \times 10^5 t_0$ (see Fig. 8).

As discussed in the previous section, the coefficients ε and α do not depend on the details of the long-time many-body interactions, while T_c does. This was already shown for the hard-sphere fluids. In order to show this even for Lennard-Jones binary mixtures, for comparison we take the simulation results by Gallo et al. [17] for a Lennard-Jones binary mixture embedded in an off-lattice matrix of soft spheres, where the average particle distance L_0 is given by $L_0 = 12.6\sigma_{AA}/1000^{1/3} = 1.26\sigma_{AA}$. In Fig. 8, the results are also shown versus $1/T$ for comparison. The simulation results are well described by the singular and the non-singular functions

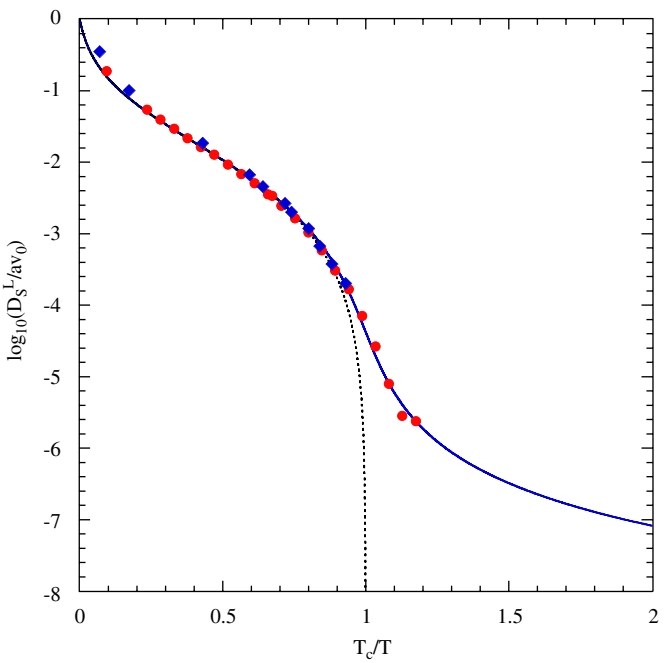

Fig. 9. (Color online) A log plot of the long-time self-diffusion coefficient D_L/av_0 versus T_c/T for two different Lennard-Jones binary mixtures. The details are the same as in Fig. 8.

given by Eqs. (13) and (14), respectively, where $\beta_c \simeq 2.9070$ ($T_c \simeq 0.3440$), $\varepsilon \simeq 46.77$, and $\alpha \simeq 2.05$. In Fig. 9, a log plot of $\hat{D}_L$ is shown versus T_c/T for both simulation results. Those results turn out to be collapsed on the non-singular master curve given by Eq. (13) with Eq. (14). Thus, one can conclude that for any systems the coefficients ε and α do not depend on the details of the many-body interactions if the main mechanisms are the same, while T_c depends on them.

In Fig. 4, the fitting values of the mean-free path $\hat{\ell}$ for the Lennard-Jones binary mixture and also those for the confined Lennard-Jones binary mixture are shown together with the results for hard-sphere fluids. Here in the binary mixture ℓ_0 is chosen as $\ell_0 = a$, while in the confined binary mixture it is chosen as $\ell_0 = (1.26/0.94)a$ since its average particle distance is $L_0 = 1.26\sigma_{AA}$ and that of the binary mixture is $L_0 = 0.94\sigma_{AA}$. Within error, those values are collapsed on the same curve as that obtained for hard-sphere fluids. Thus, the mean-free path $\hat{\ell}$ is determined by $\hat{D}_L$ only. This suggests that the dynamics in different systems becomes identical with each other at a given value of $\hat{D}_L$. We discuss this next.

4. A dynamical mapping

In this section, we discuss a dynamical mapping from one system to another at a given value of $\hat{D}_L$. As discussed in Ref. [13], the dynamics in any equilibrium systems become identical at a given value of $\hat{D}_L$. This means that $\hat{D}_L$ determines the macroscopic behavior of the systems.

We first discuss the relation between control parameters in two different systems, on which the diffusion coefficient $\hat{D}_L$ coincides to each other. Let p and p' be control parameters in two different systems. Then, by solving the following equation:

$$\frac{D_S^L(p)}{av_0} = \frac{D_S^L(p')}{av_0} \tag{20}$$

and using Eq. (7), one can find a relation between p_n and p'_n. As an example, we compare the hard-sphere fluid with 15% polydispersity with the Lennard-Jones binary mixture, where the control parameter is ϕ and $1/T$,

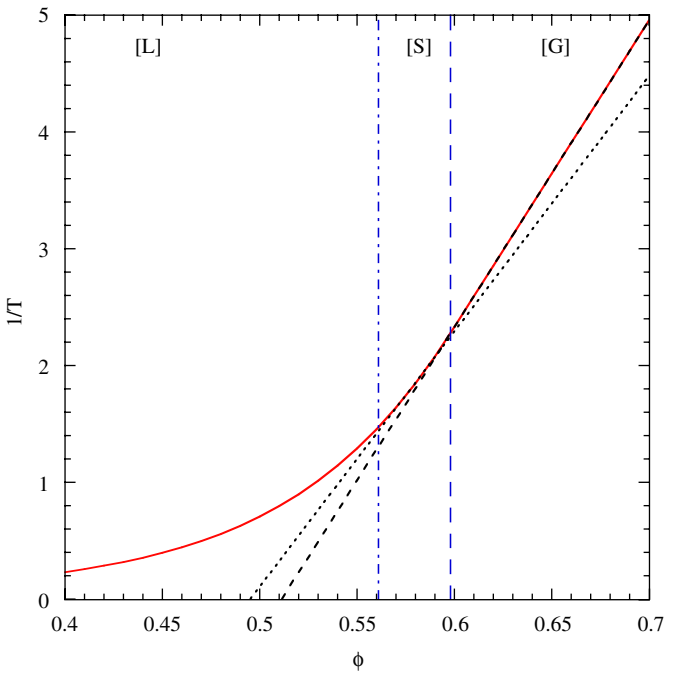

Fig. 10. (Color online) A $\beta-\phi$ iso-diffusive curve. The solid line indicates the solution of Eq. (20), the dotted line the linear line given by Eq. (21), and the dashed line given by Eq. (22). The details are the same as in Fig. 3.

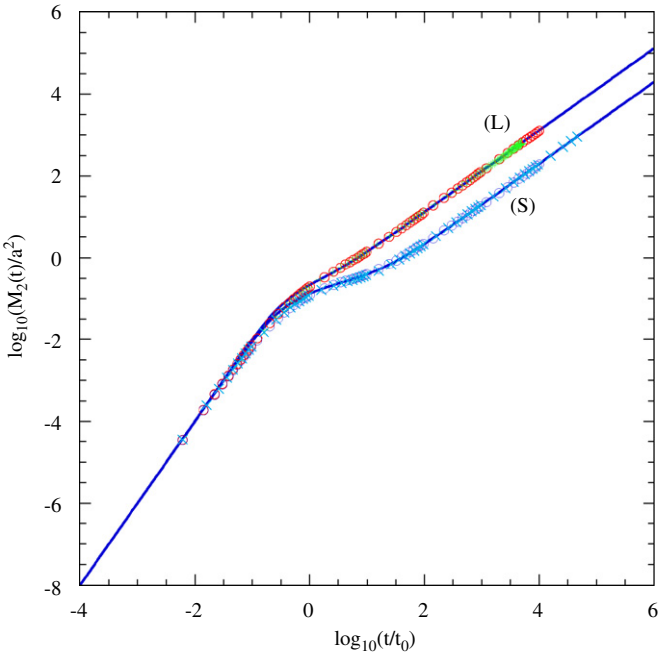

Fig. 11. A mapping of the hard-sphere fluid with $s = 0$ or $s = 0.06$ onto that with $s = 0.15$ at a given value of $\hat{D}_L$. (L) $\hat{D}_L \simeq 0.0215$: $\circ$ $s = 0.15$, $\phi = 0.51$ and $+$ $s = 0$, $\phi = 0.503$, and (S) $\hat{D}_L \simeq 0.00328$: $\circ$ $s = 0.15$, $\phi = 0.56$ and $\times$ $s = 0.06$, $\phi = 0.553$. The solid lines are the mean-field results given by Eq. (4).

respectively. In Fig. 10, the $\beta-\phi$ iso-diffusive curve is shown. In stages [S] and [G], $1/T$ obeys two different linear equations given by

$$T^{-1} = 21.86\phi - 10.82 \quad \text{for [S]}, \tag{21}$$

$$T^{-1} = 26.27\phi - 13.43 \quad \text{for [G]}. \tag{22}$$

These linear relations suggest that in two stages [S] and [G] macroscopic collective motion dominates the dynamics of the system. In any point on such a $p - p'$ curve, the dynamical behavior in two different systems are expected to become identical. We next discuss this in three cases separately.

The first case is a mapping from the hard-sphere fluid with $s = 0$ or $s = 0.06$ to that with $s = 0.15$. In Fig. 11, $M_2(t)$ is compared at two different values of $\hat{D}_L$; (L) $\hat{D}_L \simeq 0.0186$ in a liquid state [L] where $\phi = 0.51$ for $s = 0.15$ and $\phi = 0.503$ for $s = 0$, and (S) $\hat{D}_L \simeq 0.00284$ in a supercooled state [S] where $\phi = 0.560$ for $s = 0.15$ and $\phi = 0.553$ for $s = 0.06$. At each value of $\hat{D}_L$, the simulation results are collapsed on the master curve given by Eq. (4).

The second is a mapping from the confined Lennard-Jones binary mixture to the Lennard-Jones binary mixture. In Fig. 12, $M_2(t)$ is compared at two different values of $\hat{D}_L$; (L) $\hat{D}_L \simeq 5.9 \times 10^{-3}$ in a liquid state [L] where $\beta = 1.2$ ($T = 0.8333$) for the binary mixture and $\beta = 1.724$ ($T = 0.580$) for the confined mixture, and (S) $\hat{D}_L \simeq 1.023 \times 10^{-3}$ in a supercooled state [S] where $\beta = 1.7$ ($T = 0.588$) for the mixture and $\beta = 2.325$ ($T = 0.43$) for the confined mixture. In order to obtain $M_2(t)$, we have scaled it by a^2 in the binary mixture and by ℓ_0^2 in the confined mixture where $\ell_0 = (1.26/0.94)a$. This is reasonable since ℓ is scaled by ℓ_0 in the confined mixture. At each value of $\hat{D}_L$, the simulation results are then collapsed on the master curve given by Eq. (4).

The third case is a mapping from the hard-sphere fluid with $s = 0.15$ to the Lennard-Jones binary mixture. In Fig. 13, $M_2(t)$ is compared at two different values of $\hat{D}_L$; (L) $\hat{D}_L \simeq 0.0215$ in a liquid state [L] where $\phi = 0.51$ for $s = 0.15$ and $\beta = 0.8$ ($T = 1.25$), and (S) $\hat{D}_L \simeq 0.00136$ in a supercooled state [S] where $\phi = 0.570$ for $s = 0.15$ and $\beta = 1.7$ ($T = 0.588$). At each value of $\hat{D}_L$, the simulation results are collapsed on the master curve given by Eq. (4). As shown in Fig. 10, near the glass transition, both the systems are linearly related to each other through T and ϕ. This means that both in a supercooled state and in a glass state the macroscopic

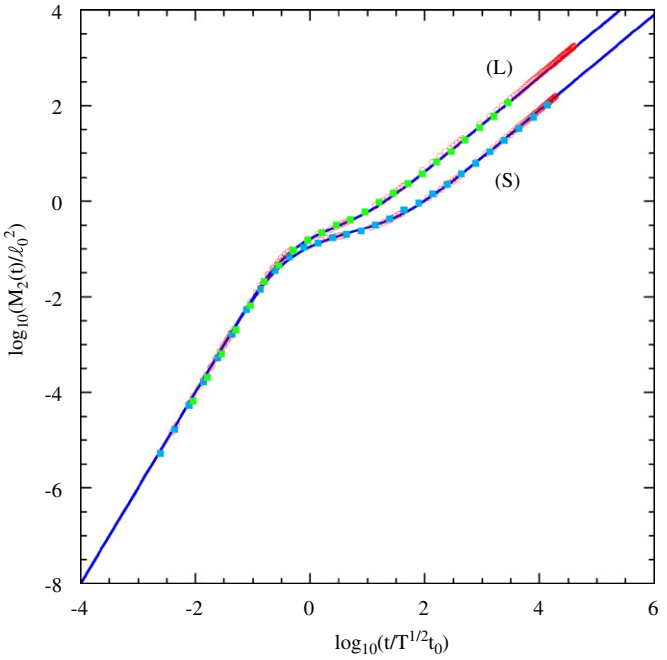

Fig. 12. A mapping of the confined Lennard-Jones binary mixture onto the Lennard-Jones binary mixture at different diffusion coefficient $\hat{D}_L$. The circles indicate the results for the Lennard-Jones binary mixtures where $\ell_0 = a$ and the boxes the confined binary mixture from Ref. [17] where $\ell_0 = (1.26/0.94)a$. (L) $\hat{D}_L \simeq 6.812 \times 10^{-3}$ at $\circ$ $\beta = 1.2$ ($T = 0.8333$) and $\square$ $\beta = 1.724$ ($T = 0.580$), and (S) $\hat{D}_L \simeq 1.181 \times 10^{-3}$ at $\circ$ $\beta = 1.7$ ($T = 0.588$) and $\square$ $\beta = 2.325$ ($T = 0.43$). The solid lines indicate the mean-field results given by Eq. (4).

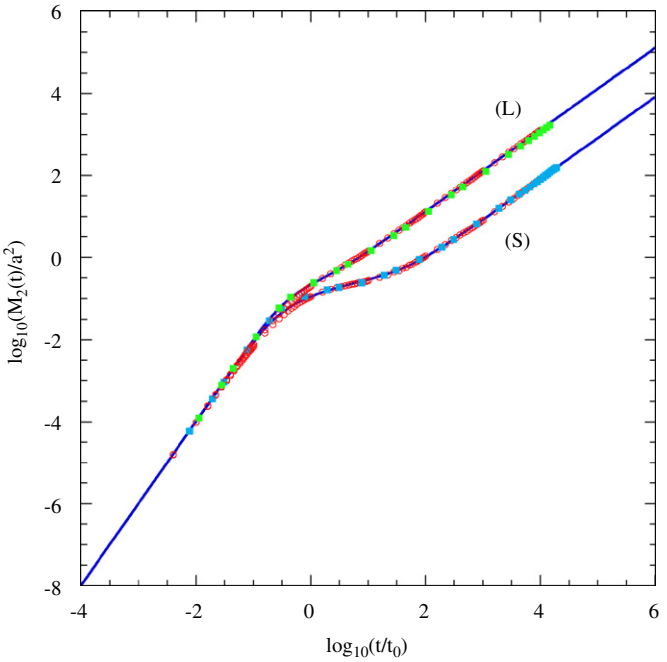

Fig. 13. A mapping of the hard-sphere fluid onto the Lennard-Jones binary mixture at different diffusion coefficient $\hat{D}_L$. The circles indicate the results for the hard-sphere fluids with $s = 15\%$ and the boxes for Lennard-Jones binary mixtures. In the binary mixture t_0 is replaced by $T^{1/2}t_0$. (L) $\hat{D}_L \simeq 2.159 \times 10^{-2}$ at $\circ$ $\phi = 0.510$ ($s = 0.15$) and $\square$ $\beta = 0.8$ ($T = 1.25$), and (S) $\hat{D}_L \simeq 1.181 \times 10^{-3}$ at $\circ$ $\phi = 0.570$ ($s = 0.15$) and $\square$ $\beta = 1.7$ ($T = 0.588$). The solid lines indicate the mean-field results given by Eq. (4).

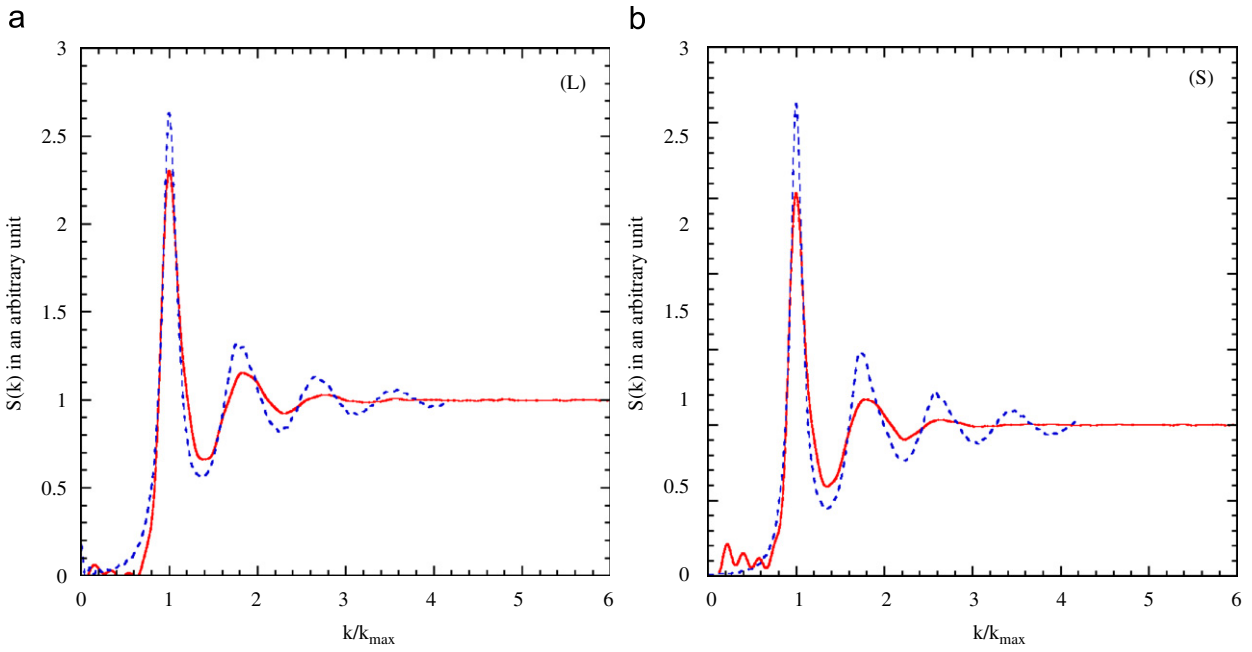

Fig. 14. (Color online) A static structure factor $S(k)$ versus k/k_{max} for different coefficients $\hat{D}_L$, where k_{max} is a first-peak position of $S(k)$. (L) $\hat{D}_L \simeq 0.0215$: the dashed line indicates the result at $\beta = 0.8$ and the solid line at $\phi = 0.510$ and $s = 0.15$, and (S) $\hat{D}_L \simeq 0.00136$: the dashed line at $\beta = 1.7$ and the solid line at $\phi = 0.570$ and $s = 0.15$.

behavior with long space-time scales in different systems becomes identical, irrespective of the details in the system. This situation is also seen in Fig. 4, where the mean-free path $\hat{\ell}$ is the same for different systems. On the $\beta-\phi$ curve, therefore, the macroscopic spatial structures in different systems are also expected to be identical. In order to see this, in Fig. 14 we show the static structure factor $S(k)$ in both states, [L] and [S]. In fact, the peak positions of the structure factors in both systems coincide with each other up to a third peak in both states, [L] and [S], although their detailed shapes are different.

5. Conclusions

By performing extensive molecular-dynamics simulations on two different glass-forming systems, hard-sphere fluids and Lennard-Jones binary mixtures, we have tested the prediction proposed by the MFT that one system can be mapped onto another near their glass transitions. This was done by checking four categories discussed in Section 1. The results are as follows:

(i) The mean-field equation (3) was shown to describe the simulation results very well, except in the glass state where the systems are not in equilibrium yet.
(ii) The mean-free path ℓ was shown to be uniquely determined by D_S^L and not to depend on the details of the systems (see Fig. 4).
(iii) The long-time self-diffusion coefficient $D_S^L(p)$ was shown to obey the singular function given by Eq. (6) partially. Then, the singular function was transformed into the non-singular function by using Eq. (7), which can describe the simulation results very well for a whole range of p. It was also shown that if the interactions are the same as each other, the coefficients α and ε do not change, while the singular point p_c depends on the details of the system. This is shown in Table 1. Hence the different simulation results are collapsed onto master curves (see Figs. 3(d) and 9).
(iv) At a given value of $D_S^L(p)$ the macroscopic physical quantities in any systems were shown to become identical with each other. Hence the macroscopic dynamics in one system can be exactly mapped onto that in another system (see Figs. 11–13). This suggests that the fragile systems can be exactly simulated by a simpler system.

Table 1
α, ε, and p_c for different systems

System	α	ε	p_c	p_β	p_g
HSS	4.86	1.0	0.5560	0.5440	0.5800
HSF(0.00)	4.86	1.0	0.5828	–	–
HSF(0.06)	4.86	1.0	0.5843	0.5538	0.5905
HSF(0.15)	4.86	1.0	0.5923	0.5611	0.5981
LJBM	2.05	46.77	2.1285	1.4797	2.2851
CLJBM	2.05	46.77	2.9070	2.0091	2.9862

HSS indicates the hard-sphere suspension (experiment), HSF(s) the hard-sphere fluid with polydispersity s (simulation), LJBM the Lennard-Jones binary mixture (simulation), and CLJBM the confined Lennard-Jones binary mixture (simulation), where $p = \phi$ for hard-sphere systems and $p = 1/T$ for Lennard-Jones systems. p_β and p_g were obtained at $\hat{D}_\beta = 2.95 \times 10^{-3}$ and $\hat{D}_g = 9.16 \times 10^{-6}$, respectively.

As discussed in the previous paper Ref. [13], we were also convinced by the simulation results that the dimensionless quantity $\hat{D}_L (= D_S^L/d_0)$ is a universal parameter to connect one glass-forming system with another near the glass transition. Hence one can predict the dynamics in fragile systems by analyzing the dynamics in simpler systems at a given value of $\hat{D}_L$. This situation also holds exactly for suspensions of colloids. Finally, it would be valuable to know whether the present approach is applicable to more exotic glasses or not. This will be discussed elsewhere.

Acknowledgments

This work was partially supported by Grants-in-Aid for Science Research with No. 18540363 from Ministry of Education, Culture, Sports, Science and Technology of Japan. Numerical computations for this work were performed on the Origin 2000 machine at the Institute of Fluid Science, Tohoku University.

References

[1] C.A. Angell, K.L. Ngai, G.B. McKenna, P.F. McMillan, S.W. Martin, J. Appl. Phys. 88 (2000) 3113.
[2] P.G. Debenedetti, F.H. Stillinger, Nature 410 (2001) 259.
[3] K.L. Ngai (Ed.), Proceedings of the Fourth International Discussion Meeting on Relaxation in Fragile Systems, J. Non-Cryst. Solids 307–310 (2002).
[4] M. Tokuyama, I. Oppenheim (Eds.), Proceedings of the Third International Symposium on Slow Dynamics in Fragile Systems, vol. CP708, AIP, New York, 2004.
[5] K. Binder, W. Kob, Glassy Materials and Disordered Solids, World Scientific, Singapore, 2005.
[6] E.R. Weeks, J.C. Crocker, A.C. Levitt, A. Schofield, D.A. Weitz, Science 287 (2000) 627.
[7] M. Tokuyama, Phys. Rev. E 54 (1996) R1062.
[8] M. Tokuyama, Phys. Rev. E 62 (2000) R5915.
[9] M. Tokuyama, Physica A 289 (2001) 57.
[10] M. Tokuyama, Physica A 315 (2002) 321.
[11] M. Tokuyama, H. Yamazaki, Y. Terada, Phys. Rev. E 67 (2003) 062403.
[12] M. Tokuyama, Physica A 364 (2006) 23.
[13] M. Tokuyama, Physica A 378 (2007) 157.
[14] W. van Megen, T.C. Mortensen, S.R. Williams, J. Müller, Phys. Rev. E 58 (1998) 6073.
[15] M. Tokuyama, I. Oppenheim, Phys. Rev. E 50 (1994) R16.
[16] W. Kob, H.C. Andersen, Phys. Rev. Lett. 73 (1994) 1376;
W. Kob, H.C. Andersen, Phys. Rev. E 51 (1995) 4626.
[17] P. Gallo, R. Pellarin, M. Rovere, Phys. Rev. E 67 (2003) 041202.
[18] M. Tokuyama, Y. Terada, J. Phys. Chem. B 109 (2005) 21357.
[19] M. Tokuyama, Y. Terada, Physica A 375 (2007) 18.
[20] W.S. Jodrey, E.M. Tory, Phys. Rev. A 32 (1985) 2347.
[21] J. Tobochnik, P.M. Chapin, J. Chem. Phys. 88 (1988) 5824.
[22] Y. Song, R.M. Stratt, E.A. Mason, J. Chem. Phys. 88 (1988) 1126.
[23] M.D. Rintoul, S. Torquato, Phys. Rev. Lett. 77 (1996) 4198.